Available online at www.sciencedirect.com
ScienceDirect
Applied Thermal Engineering 28 (2008) 975–987
APPLIED THERMAL ENGINEERING
www.elsevier.com/locate/apthermeng

# Theoretical and experimental evaluation of an indirect-fired GAX cycle cooling system

V.H. Gómez [a,*], A. Vidal [a], R. Best [b], O. García-Valladares [b], N. Velázquez [c]

[a] Posgrado en Ingeniería, Energía, Universidad Nacional Autónoma de México, Privada Xochicalco S/N, Apdo. Postal 34, 62580 Temixco Morelos, México
[b] Centro de Investigación en Energía, Universidad Nacional Autónoma de México, Privada Xochicalco S/N, Apdo. Postal 34, 62580 Temixco Morelos, México
[c] Instituto de Ingeniería, Universidad Autónoma de Baja California, Calle de la Normal S/N, Insurgentes Este, 21280 Mexicali, BC, México

Received 8 July 2006; accepted 26 June 2007
Available online 3 July 2007

**Abstract**

A theoretical and experimental evaluation of an indirect-fired GAX-Prototype Cooling System (GAX-PCS), using ammonia–water as the working fluid, is presented. The GAX-PCS was designed for a cooling capacity of 10.6 kW (3 tons). A simulation model was developed, calibrated and validated with experimental values in order to predict the performance of the system outside the design parameters. Experimental results were obtained using thermal oil, at temperatures from 180 to 195 °C, as heating source. An internal heat recovery in the system of ~55% with respect to the total heat supplied in the generator was obtained. Also the performance of the GAX absorption system, integrated to a micro gas turbine (MGT) as a cogeneration system was simulated. Overall efficiencies for the cogeneration system from 29% to 49% were obtained for cooling loads from 5 kW to 20 kW, respectively. With the theoretical and experimental study of the proposed cycle, it is concluded that the GAX-PCS presents potential to compete technically in the Mexican air conditioning market.


*Keywords:* Ammonia–water; Absorption; Waste heat; Air conditioning; Microturbine

## 1. Introduction

Nowadays, there is a worldwide interest in energy systems that can work recovering waste heat or that use renewable energy and less primary energy from fossil fuel combustion, which products contribute to climate change and the greenhouse effect.

The Generator Absorber heat eXchange (GAX) absorption cooling cycle has a great potential to decrease electrical energy consumption for air-conditioning in the residential and small commercial sectors. An indirect-fired system also offers the possibility of using alternative thermal energy technologies such as advanced concentrating collectors in high beam irradiance areas, as the northern part of Mexico, hybrid systems (i.e. solar–natural gas) or to make use of waste heat from microturbines, increasing the efficiency of cogeneration systems [1–3].

The absorption systems typically work with a binary mixture, the refrigerant and the absorbent (e.g. ammonia–water, lithium bromide–water), these mixtures substitute the conventional refrigerants (CFCs and HCFCs) which are responsible in a part of the global warming and the depletion of the stratospheric ozone layer. A common binary mixture used in absorption systems is ammonia–water, which is environmentally friendly with a lower cost.

The traditional single effect ammonia–water system reaches typically a coefficient of performance ($COP_{th}$) of around 0.5–0.6 [4,5]. However, it can be reach up to 0.75 for water cooled systems (with water condensation temperatures from 20 to 25 °C) and radiant ceiling cooling applications (evaporation temperature from 5 to 10 °C). The lithium bromide–water systems with a $COP_{th}$ around of

* Corresponding author. Tel.: +52 55 56229739; fax: +52 55 56229791.
*E-mail address:* vhge@cie.unam.mx (V.H. Gómez).

1359-4311/$ - see front matter 
doi:10.1016/j.applthermaleng.2007.06.027

**Nomenclature**

| | |
|---|---|
| AB | absorber |
| AC | air compressor |
| AHX | absorber heat exchangers |
| CC | combustion chamber |
| CO | condenser |
| $COP_{th}$ | thermal coefficient of performance |
| $COP_{th\text{-}aux}$ | thermal coefficient of performance with parasite power auxiliary |
| EC | economizer |
| EG | electric generator |
| EV | evaporator |
| $Ex_{FU}$ | fuel exergy |
| F | air filter |
| FR | flow ratio |
| GAX | generator–absorber heat exchangers |
| PCS | prototype cooling system |
| GE | generator |
| GHX | generator heat exchangers |
| $m$ | mass flow (kg/min) |
| MGT | micro gas turbine |
| $P$ | pressure (bar) |
| PR | precooler |
| $Q$ | heat rate (kW) |
| $Q_{EL}$ | electrical load (kWe) |
| $Q_{FU}$ | fuel energy (kW) |
| $Q_{ir\text{-}ab}$ | internal heat recovery in the absorber (kW) |
| $Q_{ir\text{-}ge}$ | internal heat recovery in the generator (kW) |
| RE | rectifier |
| $R_{Ex}$ | exergy efficiency |
| REG | regenerator |
| SP | solution pump |
| $T$ | temperature (°C) |
| TUR | turbine |
| TV | throttle valve |
| $T_0$ | reference temperature (°C) |
| $W$ | power (kW) |
| $\eta_{I,cog}$ | first law cogeneration efficiency (%) |
| $\eta_{II,cog}$ | second law cogeneration efficiency (%) |

0.7–0.8 for the same applications [4]. The GAX cycle is a system that provides the highest coefficient of performance of any single effect absorption cycle. Theoretical studies report for GAX systems $COP_{th}$ 30% higher than single effect cycles [4,5]; recently some experimental studies of GAX cycle for air-conditioning and refrigeration have been reported [6,7]. The GAX technology was theoretically developed by Altenkirch in 1913 [4], but the first prototype working with natural gas was constructed in 1980. This technology is nowadays a reality, but research and developed in this subject continues. In the last two decades important contributions in order to increase the performance of these cycles has been achieved. For example, the GAX cycle with the addition of a pump, to recycle part of the solution from the absorber to the generator in order to equalise the quantities of heat exchanged, is known as Branched GAX cycle (BGAX) [8]; different types of recirculations have been proposed, reporting increases in the $COP_{th}$ up to 30% higher than the simple GAX cycle. Many other advanced cycles are based on the principles developed by Altenkirch, such as the Vapour Exchange GAX cycle (VXGAX) [9], Multi GAX cycle (MGAX) [10], the Polybranched GAX (PBGAX) [10], and Regenerative GAX cycle (RGAX) [11], amongst other. Kang et al. [12] proposed the waste heat driven GAX cycle (WGAX) in order to reduce the required temperature levels in the generator and therefore, opening the possibility of utilising waste heat and avoiding corrosion problems. In the Centro de Investigación en Energía of UNAM a GAX absorption prototype has been designed and constructed for a nominal capacity of 10.6 kW (3 ton) [13]. In this type of systems the priority is the internal energy integration, which increases the cycle efficiency. The system was designed to be air-cooled for ambient temperatures of 40 °C, at these conditions a theoretical coefficient of performance ($COP_{th}$) of 0.82 including electricity consumption was numerically calculated. In this paper, a comparison between theoretical results and experimental results obtained with the GAX-PCS working under different conditions will be presented.

## 2. Methodology

### 2.1. GAX effect

The GAX cycle conserves the essential elements of a single effect water–ammonia cooling absorption cycle: generator (GE), rectifier (RE), absorber (AB), condenser (CO), precooler (PR), economizer (EC), evaporator (EV), throttled valves (TV) and a solution pump (SP). The difference between a traditional single effect cycle and GAX is the internal heat recovery; part of the absorption heat is recuperated by the generator, which leads to a decrease of the thermal energy supply in this device, increasing the $COP_{th}$ of the system. In order to obtain this effect it is necessary to add to the system a pair of heat exchangers and a pump if a hydronic loop for the heat transfer is used. Fig. 1(a) and (b) shows the schematic comparison of a traditional single effect absorption system and the GAX system.

### 2.2. Description of GAX-PCS

The Hybrid GAX-PCS, have the same essential elements of a single effect water–ammonia cooling absorption cycle.

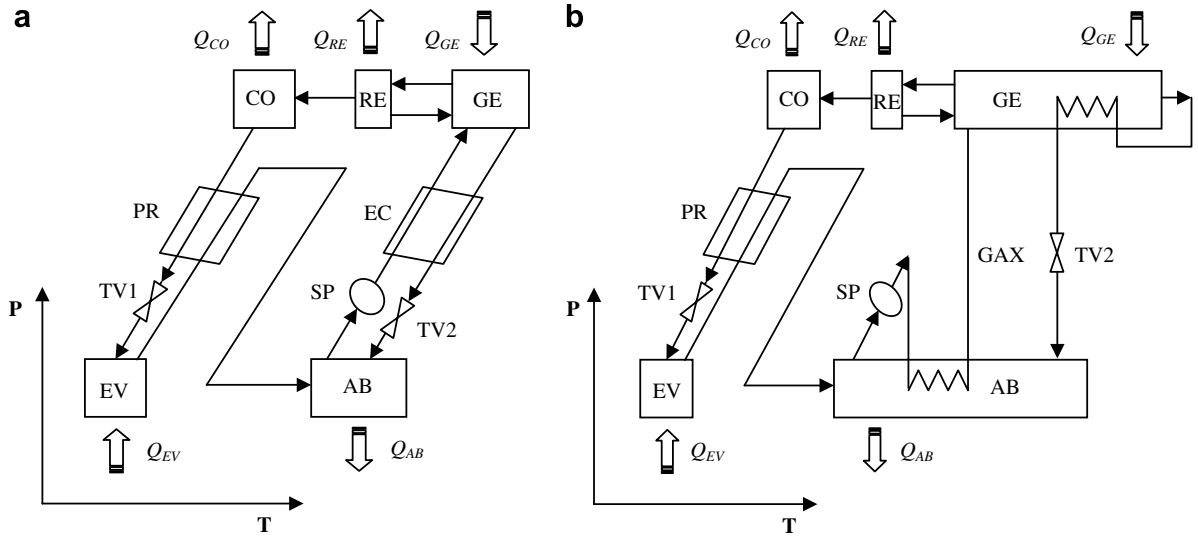


Fig. 1. (a) Single effect traditional absorption cooling cycle; (b) GAX absorption cooling cycle.

The rectifier is placed at the top of the generator, to make an integrated generator–rectifier (GE–RE) column. The GAX section of the generator is placed in the top of the absorber in order to integrate the absorber-GAX (AB-GAX) column, as shown in Fig. 2. Both, GE–RE and AB-GAX columns are separated in sections for higher energy integration, obtaining an important reduction in the heat supply to the generator and also a reduction in the heat rejected in the absorber. These columns are of the falling film type; they were manufactured with annular finned tubes in order to improve the heat transfer. The condenser, precooler and evaporator are compact shell and tube heat exchangers. Fig. 3(a) shows the generator–rectifier and absorber-GAX columns of the GAX-PCS cooling system, and Fig. 3(b) shows the condenser, precooler and evaporator, as well as the solution pump [14]. At this experimental stage, the system only used thermal oil to drive the generator, which was heated by a 24 kW electrical resistance. At a following stage it will be driven by a hybrid energy source (LP gas–solar) using an indirect-fired burner and high efficiency solar collectors. The energy indicators selected to evaluate the operation of the absorption cooling system were: the thermal coefficient of performance ($COP_{th}$) defined by Eq. (1), the thermal coefficient of performance including the parasitic power required for pumps and fans of the system ($COP_{th\text{-}aux}$) Eq. (2), and the flow ratio (RF), defined by Eq. (3), using subscripts with reference to Fig. 2

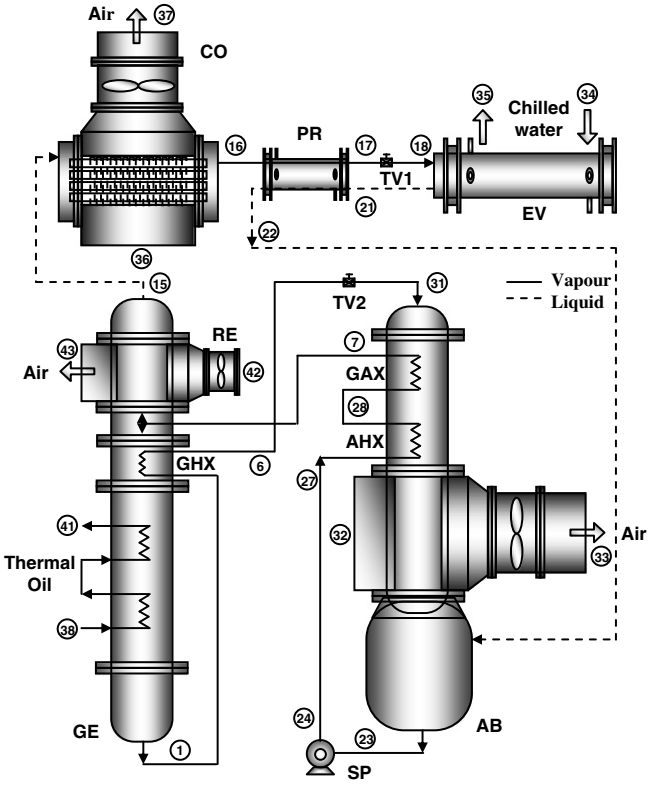


Fig. 2. Schematic diagram of GAX absorption cooling prototype.

$$COP_{th} = \frac{Q_{EV}}{Q_{GE}} \tag{1}$$

$$COP_{th\text{-}aux} = \frac{Q_{EV}}{Q_{GE} + W_{SP} + W_{AB} + W_{CO} + W_{RE}} \tag{2}$$

$$FR = \frac{\dot{m}_7}{\dot{m}_{15}} \tag{3}$$

### 2.3. Description of the GAX-PCS coupled to the micro gas turbine (MGT)

The cogeneration or simultaneous production of useful heat and power in a thermal system often involving a turbine, in which a fuel is burnt to produce hot gases to drive a turbine coupled to an electric generator. The thermal energy of the exhaust gases is recovered to drive an absorption cooling system before being rejected to the

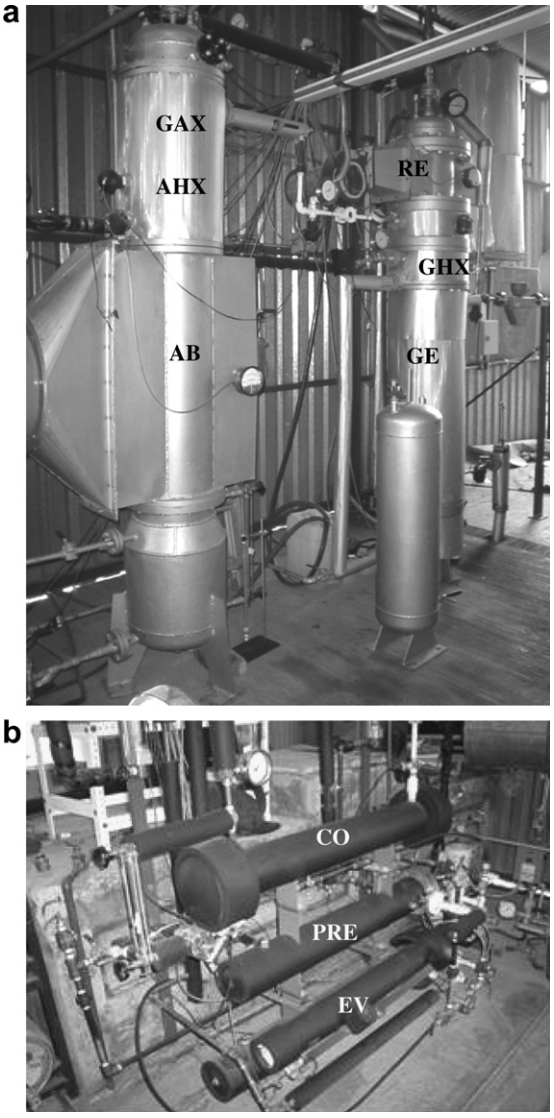


Fig. 3. (a) Generator–rectifier and absorber-GAX columns of the GAX cycle, (b) condenser, precooler and evaporator equipments of the absorption cooling system.

environment. The theoretical cogeneration system presented in this paper utilises a MGT as the primary power generation system, to which the generator of a GAX-PCS was coupled in two different configurations, as shown in Fig. 4(a) and (b). The first configuration proposed in Fig. 4(a), with direct use of the exhaust gases in the GAX generator includes: (A) the MGT and (B) the GAX-PCS. The second configuration proposed in Fig. 4(b), includes: (A) the MGT, (B) the heat recovery system, with a heat exchanger between the thermal oil and the exhaust gases and (C) the GAX-PCS. The MGT selected for this study had a nominal capacity of 30 kWe. Table 1 shows the main characteristics of the MGT, operating in steady state conditions. More specific data of the exhaust gases at different conditions have been reported [15].

The overall system efficiency can be calculated from the ratio of the cooling load plus electrical load to the input fuel energy to the cogeneration system, as expressed by Eq. (4) [16]:

$$\eta_{\mathrm{I,cog}} = \frac{Q_{\mathrm{EV}} + Q_{\mathrm{EL}}}{Q_{\mathrm{FU}}} \tag{4}$$

The second law efficiency given by Eq. (5) considers that the combustion exergy is the same for both cogeneration cases considered, however, due to the considerations for the thermal oil case, where the evaporation load and the output oil temperature are fixed, the irreversibilities due to heat transfer between the exhaust gases and the thermal oil are not reflected in the values obtained by the second law, but they appear in the evaporation load. Due to this, the evaporator load is lower in the thermal oil case, where the fuel exergy ($\mathrm{Ex_{FU}}$) is defined by [17,18] and ($R_{\mathrm{Ex}}$) is the combustion exergy efficiency and its value is around 1 depending on the type of fuel that is used. Values of $R_{\mathrm{Ex}}$ can be obtained from [19]. For this analysis, a value of $R_{\mathrm{Ex}}$ of 0.95 has been considered for the propane–butane mixture:

$$\eta_{\mathrm{II,cog}} = \frac{-Q_{\mathrm{EV}}(1 - T_0/T_{\mathrm{EV}}) + Q_{\mathrm{EL}}}{\mathrm{Ex_{FU}}} = \frac{-Q_{\mathrm{EV}}(1 - T_0/T_{\mathrm{EV}}) + Q_{\mathrm{EL}}}{R_{\mathrm{Ex}} \cdot Q_{\mathrm{FU}}} \tag{5}$$

For evaporator temperatures $T_{\mathrm{EV}}$ below ambient temperature the Carnot factor $(1 - T_0/T_{\mathrm{EV}})$ takes negative values. Due to this the first term of Eq. (5) has a negative sign in order to add the exergy produced by cooling with the exergy produced by the turbine.

### 2.4. GAX cycle numerical simulation

The simulation model in this work differs from the model developed by Herold et al. [8] as it has special characteristics mentioned in Section 2.2. Also the model was validated and adjusted with the experimental results obtained with the prototype. However, the model can be modified for different working conditions for other GAX cycles.

The ASPEN PLUS process simulator was used in order to predict the behavior of the GAX system in the generation temperature range from 180 to 220 °C, as well as the performance of the microturbine in steady state applications. The Redlich–Kwong–Soave (RKS), Braun K10 (BK-10) and Peng–Robinson–Boston–Matias (PR–BM) equations of state were selected to calculate the thermodynamic properties of the ammonia–water mixture, the thermal oil and the combustion gases, respectively, because it showed good agreement with the technical literature [20]. Specifically, ammonia–water properties have been compared with NIST database [21] obtaining differences of less than 5%. The average boiling point, molecular weight and the specific gravity values were introduced in the simulator to calculate the thermophysical properties of the thermal oil, because they were not provided in the database [22].

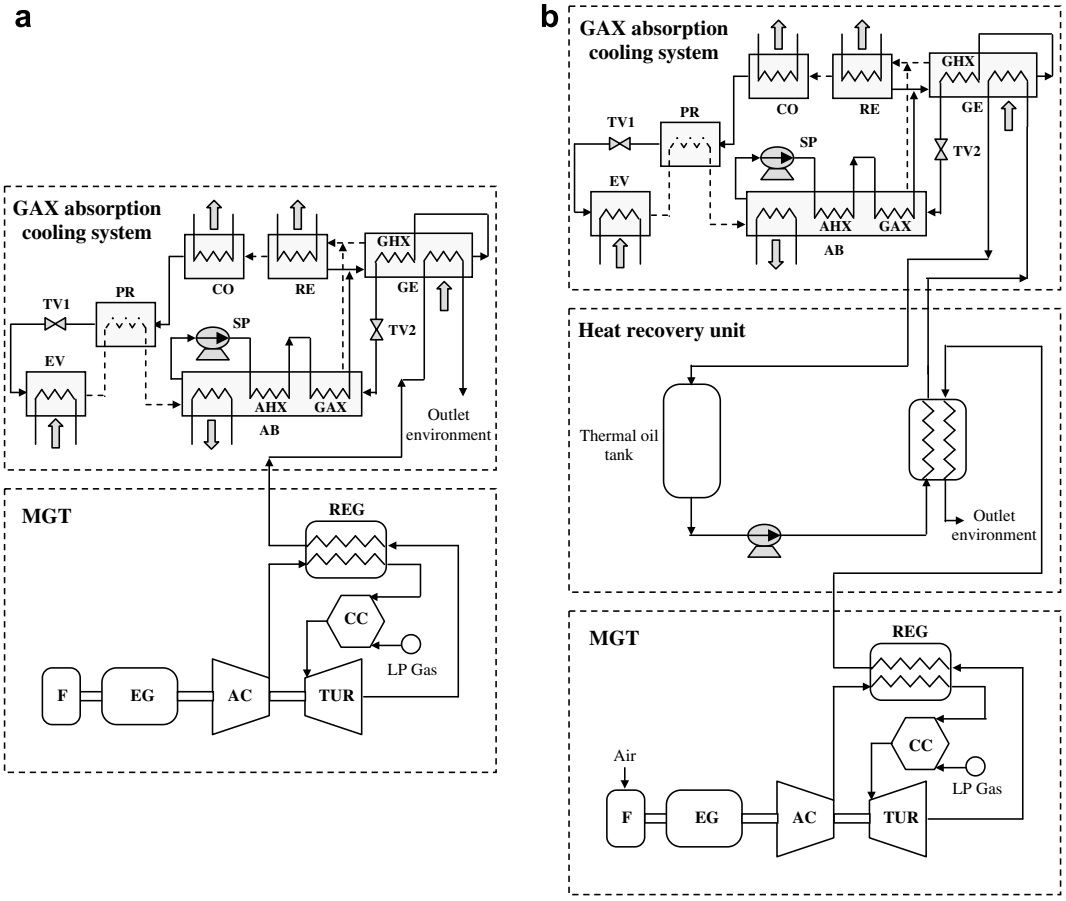


Fig. 4. Schematic diagram of GAX-PCS coupled with (a) MGT; (b) MGT and heat recovery system.

Table 1
Characteristics of the micro gas turbine

| Parameters | Units | Description |
|---|---|---|
| Volumetric flow rate | $m^3$/min | 14.4 |
| Mass flow rate | kg/h | 0.264 |
| Nominal electrical power | kWe | 30.0 |
| Nominal thermal power | kW | 23.4 |
| Fuel flow at full load | MJ/h | 374.5 |
| Exhaust gas temperature | °C | 293.7 |

In the simulation results, the key parameters such as, FR and temperature lift were analyzed in detail because these parameters have a close relation with the GAX operation and affect directly the $COP_{th}$ values. The following parameters and assumptions were used in the GAX absorption cooling system simulations: isentropic efficiency of the pump, 80%; mechanical and electric efficiency, 96%; minimum temperature difference for each one of the heat exchangers, 10 °C and a total drop pressure of 4% of the total pressure in the system. These values were validated with the experimental test. The following parameters were used in the MGT simulations: isentropic and mechanical efficiency of the compressor, 74% and 89%, respectively; compression ratio, 3.35; hot stream outlet temperature approach in the regenerator, 93 °C; isentropic and mechanical efficiency of the turbine, 86% and 97.4%, respectively; turbine discharge pressure, 1 bar. More details of the MGT simulation are reported by [15].

## 3. Experimental testing of the GAX system

The procedure developed to characterize and to evaluate the GAX-PCS was carried out by means of experimental tests taking the values obtained from the simulations as initial conditions. Thermal oil temperature was varied from 180 to 195 °C at the entrance of the generator–rectifier column to predict the thermal and fluid dynamic behavior of the system at this range. These experimental results were used also in order to know the mass flow rate of the different loops of the system and to compare them with the numerical results obtained by the theoretical model.

Once the system has reached the steady state, the variable adjust sequence was started. The register and store of these variables was carried out by a data acquisition system and a personal computer. Temperature measurements were collected from RTD (PT-100) probe with accuracy of ±0.15 °C, pressure values were obtained from piezoelectric transducers with an accuracy of ±0.2 bar, the mass flow measurements were obtained from Coriolis sensors with accuracy of ±0.1% and electromagnetic turbine sensors

with an accuracy of ±0.3%, while the concentration measurements of ammonia–water, weak and strong solution were obtained by chemical titration with an uncertainty of ±4%.

## 4. Results and discussion

### 4.1. Experimental result of the GAX prototype cooling system

The experimental conditions operating with thermal oil presented higher than expected heat losses that resulted in heating oil temperatures entering the generator of around 192 °C, below the design generator temperature of 225 °C. Heat losses in flanges and in the insulated piping as well as a larger than required hot oil storage tank were the main reasons for the large heat losses quantified at around 20%. To compensate these heat losses, a higher heating oil flow rate than the design value was used, that caused an increase in the heat duty. In the experimentation, the pressure in the low pressure side of the system was higher than the design value; this was a consequence of a bad distribution of the solution in the falling film absorber which did not perform as expected. This increased the evaporation pressure, and as a consequence the evaporator temperature could not be reduced to produce chilled water temperature to the design value of 10 °C. This also limited the cooling capacity of the prototype to values of around 7.1 kW against the design value of 10 kW. As a consequence, the internal heat exchange in the GHX, AHX and GAX heat exchangers was lower than expected. However, although the prototype was working below design conditions, the internal heat integration reached values of up to 6.58 kW (55.7% of the heat supplied to the generator).

Fig. 5 shows the temperature profiles of the weak solution after 25–30 min, when the system was stabilized. Fig. 5, also shows the internal heat recovery of 2.32 kW in the GHX section through the heat exchange of the weak solution flow.

Fig. 6 shows the temperature profiles of the strong solution flow when it passes through both the AHX and GAX sections, where the temperature increases in 12 and 24 °C, respectively; due to the internal heat recovery of 4.26 kW, which help to increase the cycle efficiency.

Fig. 7 shows the experimental behavior of the mass flow ratio and the circulation ratio of the GAX system according to the temperature difference between the condenser and the evaporator (cycle lift). It can be seen from Fig. 7, that as the lift increases, a higher strong solution mass flow is required to feed the generator in order to produce the same refrigerant flow.

Fig. 8 shows the way the experimental $COP_{th}$ increases, when the temperature of the thermal oil, supplied to the generator, is increased.

### 4.2. Comparison of the numerical data with experimental results of the GAX prototype cooling system

Table 2 shows the comparison of the results of the 7.1 kW (2 tons) case for the GAX-PCS, obtained numerically and experimentally, the values and uncertainties of experimental data are reported according to Verma et al. [23]. The results presented were carried out in steady state conditions when the system was stabilized. The column labeled "simulation" represents a model from a numerical simulation. According to the values obtained by the numerical simulation against the experimental results presented in Table 2, it is concluded that the model acceptably represents the experimental working conditions and can be

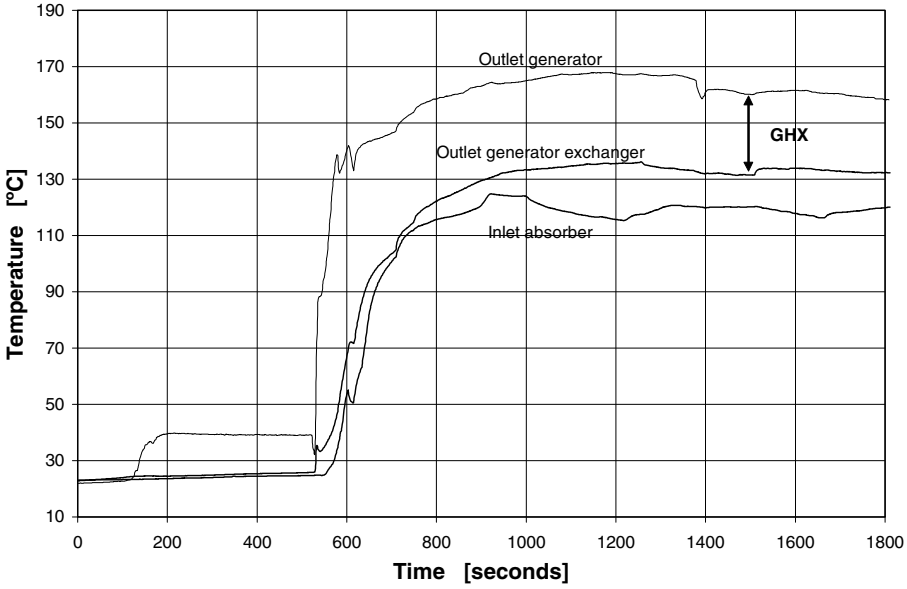


Fig. 5. Experimental weak solution temperature profiles.

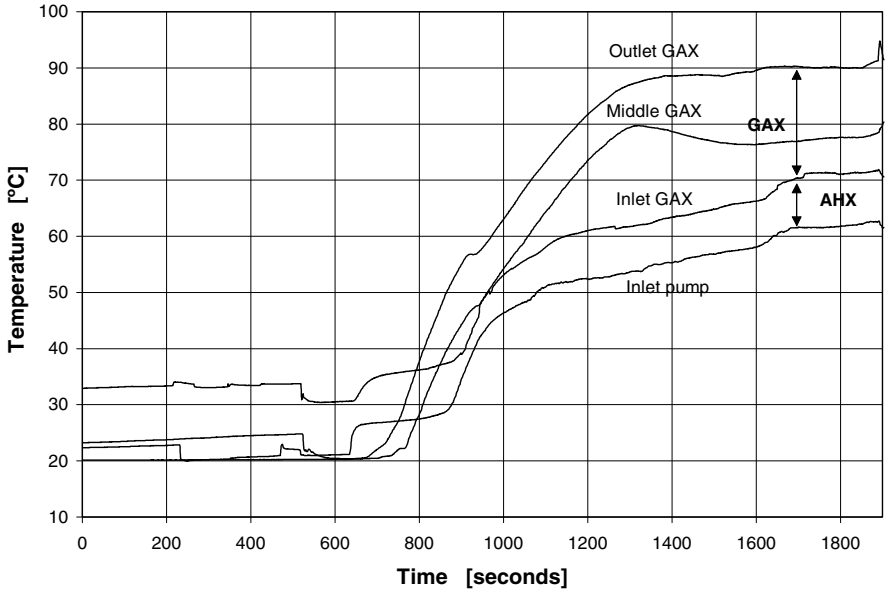


Fig. 6. Experimental strong solution temperature profiles.

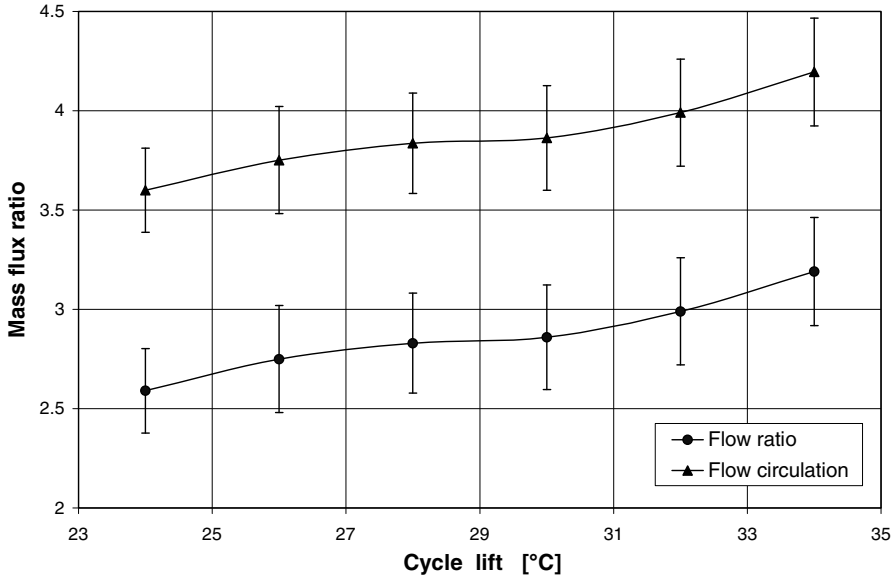


Fig. 7. Experimental mass flux ratios versus cycle lift.

used as an important tool in order to design and to optimize these systems.

Table 3 compares the experimental heat loads for each component of the GAX-PCS, to the heat loads calculated with the simulation program. The experimental results presented are average values for a series of experiments where steady state was reached and the cooling load remained constant. The generator heat load for the numerical simulation was adjusted to the experimental value, as no heat losses are considered in the theoretical model.

The required experimental generation heat load was of 11.81 kW. In order to generate the 11.81 kW it was required to circulate 10 LPM of thermal oil through the generator. The heating oil was supplied at around 195 °C and exits at 165 °C, so a real temperature difference of 30 °C in stable conditions was encountered. The temperature of the heating oil was below the expected design values due to high heat losses.

The cooling load obtained in the simulation was similar to the 7.1 kW obtained experimentally, resulting from a similar temperature difference in the chilled water. The chilled water flow rate was fixed at 15 LPM for both cases and the refrigerant vapour fraction after the expansion valve was fixed for the simulation at 5%.

The condenser heat load removed in the simulation was again very similar to the experimental value; the difference

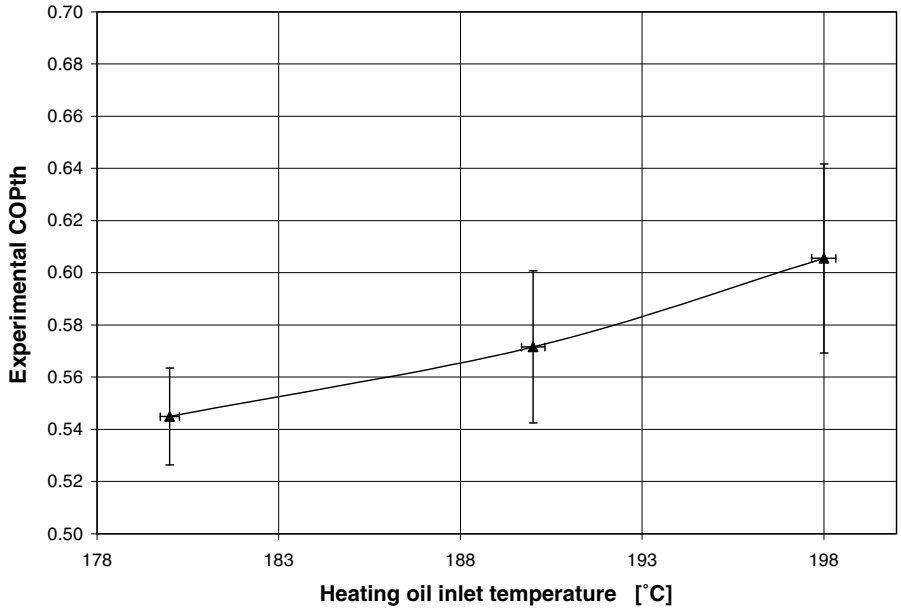


Fig. 8. Experimental COP versus heating oil inlet temperature.

Table 2
Comparison between simulation and experiment values of GAX cooling system

| Parameters (Point) | Units | Simulation | Experimental (value ± s.d.) |
|---|---|---|---|
| *Ammonia concentrations* | | | |
| Weak solution $NH_3$ fraction (1) | % | 17.00 | $17.15 \pm 0.32$ ($n = 5$) |
| Strong solution $NH_3$ fraction (23) | % | 43.50 | $42.22 \pm 0.57$ ($n = 5$) |
| Refrigerant $NH_3$ fraction (15) | % | 99.21 | $99.10 \pm 0.13$ ($n = 5$) |
| *Pressures* | | | |
| Generator | bar | 20.00[a] | $19.95 \pm 0.45$ ($n = 64$) |
| Condenser | bar | 19.96 | $19.90 \pm 0.27$ ($n = 64$) |
| Evaporator | bar | 6.00[a] | $6.20 \pm 0.12$ ($n = 64$) |
| *Flow rates* | | | |
| Refrigerant (15) | kg/min | 0.36 | $0.35 \pm 0.006$ ($n = 64$) |
| Chilled water (34) | kg/min | 15.00[a] | $15.00 \pm 0.25$ ($n = 64$) |
| *Temperatures* | | | |
| Inlet evaporator (34) | °C | 18.77 | $22.10 \pm 0.09$ ($n = 64$) |
| Outlet evaporator (35) | °C | 11.76 | $15.33 \pm 0.06$ ($n = 64$) |
| Heating oil inlet GE (38) | °C | 190.00[a] | $192.55 \pm 0.34$ ($n = 64$) |
| Outlet rectifier (15) | °C | 81.00 | $82.20 \pm 0.20$ ($n = 64$) |
| Outlet throttled valve (18) | °C | 9.70 | $11.00 \pm 0.07$ ($n = 64$) |
| *Cycle performance* | | | |
| $COP_{th}$ | | 0.61 | $0.58 \pm 0.05$ ($n = 64$) |
| $COP_{th\text{-}aux}$ | | 0.57 | $0.53 \pm 0.025$ ($n = 64$) |
| Circulation ratio | | 2.51 | $2.63 \pm 0.028$ ($n = 64$) |
| Flow ratio | | 3.51 | $3.63 \pm 0.028$ ($n = 64$) |
| Cooling load | kW | 7.30 | $7.10 \pm 0.15$ ($n = 64$) |

*n*: number of data; s.d. standard deviation.
[a] Input value.

was mainly due to the 2 °C subcooling encountered in the experimental work against the saturation conditions considered in the simulation.

Although the heat load extracted in the air cooled absorber have similar values, the experimental pressure was 6.2 bar against the 6.0 bar obtained in the simulation. This results from a poor operation of the absorber and the pressure increase suggests ammonia vapour accumulation in the absorber column and a deficient distribution of the falling film weak solution which affected the absorption process.

The experimental rectifier heat load rejected in the rectifier was 4.35% higher than the simulation value; this was the heat load with the highest difference, all the other values were below this difference.

Table 3
Comparison between simulation and experimental values of component heat loads

| Parameters | Units | Simulation | Experimental | % Difference |
|---|---|---|---|---|
| $Q_{GE}$ | kW | 11.81* | 11.81 | – |
| $Q_{EV}$ | kW | 7.30* | 7.10 | 2.74 |
| $Q_{AB}$ | kW | 9.23 | 9.21 | 0.22 |
| $Q_{CO}$ | kW | 6.65 | 6.60 | 0.75 |
| $Q_{RE}$ | kW | 2.30 | 2.40 | 4.35 |
| $Q_{PR}$ | kW | 0.90 | 0.87 | 3.33 |
| $Q_{ir\text{-}ab}$ | kW | 4.10 | 4.26 | 3.90 |
| $Q_{ir\text{-}ge}$ | kW | 2.25 | 2.32 | 3.11 |

$Q_{ir\text{-}ab}$ = Internal heat recovery in absorber.
$Q_{ir\text{-}ge}$ = Internal heat recovery in generator.
* Input value.

The internal heat recovery obtained in the simulation for the generator and absorber columns is consistent with the simulation values. Figs. 5 and 6 show the experimental temperature profiles of the strong ammonia solution and the weak ammonia solutions as they exchange heat at steady state conditions in the GHX and AHX–GAX sections, respectively. The heat recovered in the internal heat exchange was of 6.58 kW, which represents 55.7% of the total heat added to the generator.

As a result of the similarity of the heat loads, the experimental $COP_{th}$ of 0.58 is similar to the theoretical value of 0.61. The experimental value can be increased by reducing the heat losses to the ambient that can reach up to 20% of the heat added to the generator.

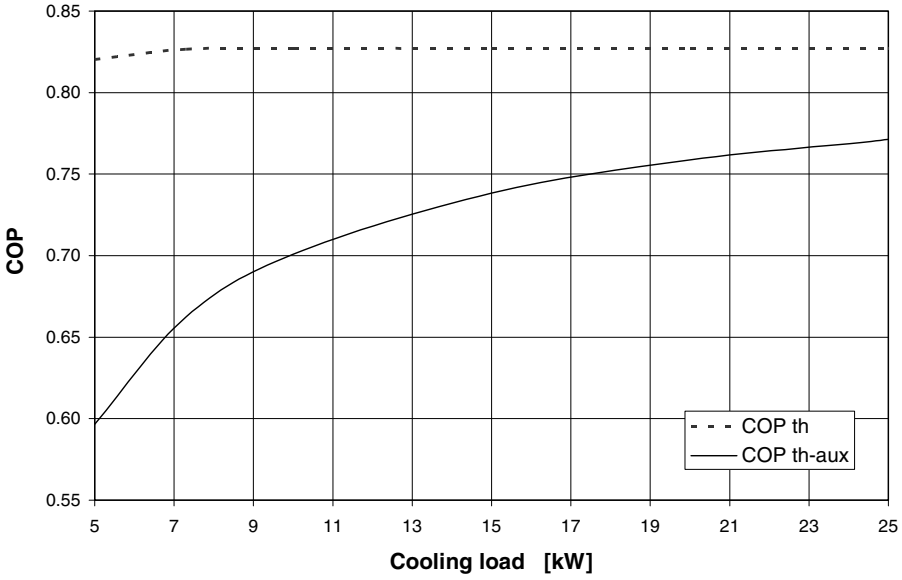


Fig. 9. Theoretical $COP_{th}$ and $COP_{th\text{-}aux}$ versus cooling load for first arrangement.

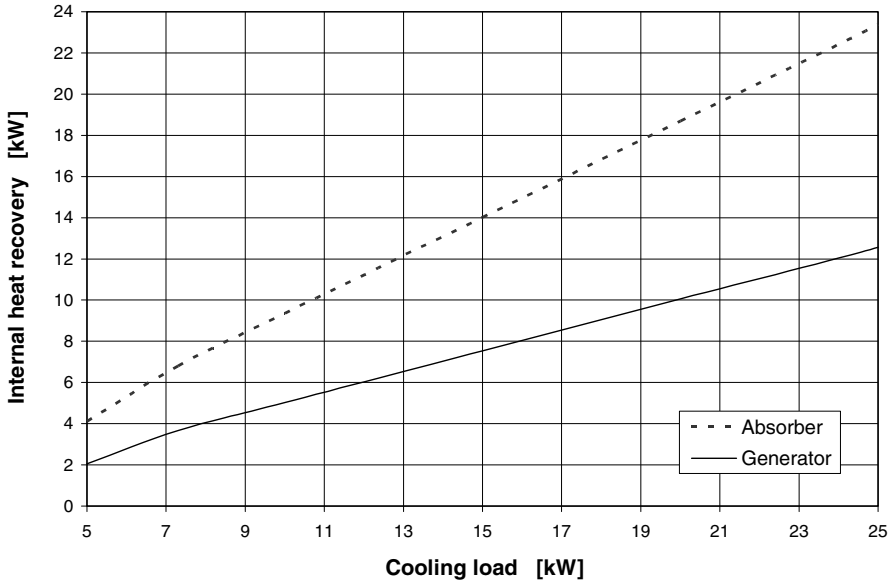


Fig. 10. Theoretical internal heat recovery versus cooling load for first arrangement.

### 4.3. Simulation of the operation of the GAX-PCS coupled to a selected MGT

Two configurations were analyzed, firstly the configuration shown in Fig. 4(a), where the exhaust gases enter directly to the generator heat exchanger. Secondly, the configuration shown in Fig. 4(b), where the hot gases exiting the MGT enter a recuperator heat exchanger to heat the thermal oil that will then enter the generator of the GAX absorption system. In both cases the cooling load was varied from a minimum value of 5 kW up to the maximum possible cooling capacity as a function of the available heat in the microturbine exhaust gases. The simulation was made considering no heat losses to the ambient for both configurations described. Fig. 9 shows the theoretical values of the coefficient of performance for cooling ($COP_{th}$) as well as the coefficient of performance including the parasitic power required for pumps and fans ($COP_{th\text{-}aux}$) for the GAX system operating from 5 to 25 kW of cooling capacity, which is the maximum cooling capacity obtained for configuration 4(a). It can be seen that as the cooling load increases the value of the $COP_{th}$ tends to be stable around 0.81–0.82, however, $COP_{th\text{-}aux}$ increases from 0.59 to 0.77 due to a higher cooling load, although the parasitic consumption also increases. The internal heat exchange in the GAX system increases significantly both in the absorber $Q_{ir\text{-}ab}$ and in the generator $Q_{ir\text{-}ge}$ as Fig. 10, shows. Consequently, this brings lower energy consumption in

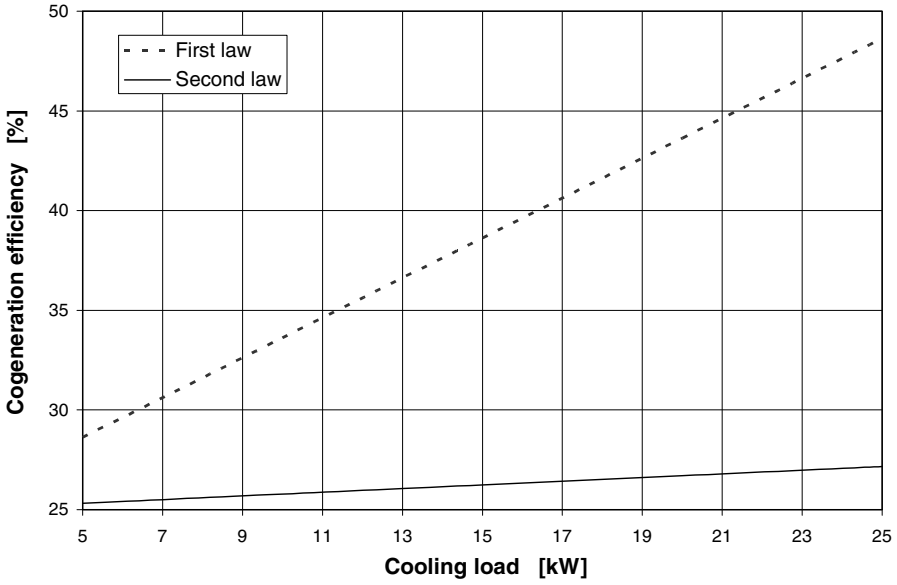


Fig. 11. Theoretical first and second law cogeneration efficiencies versus cooling load for first arrangement.

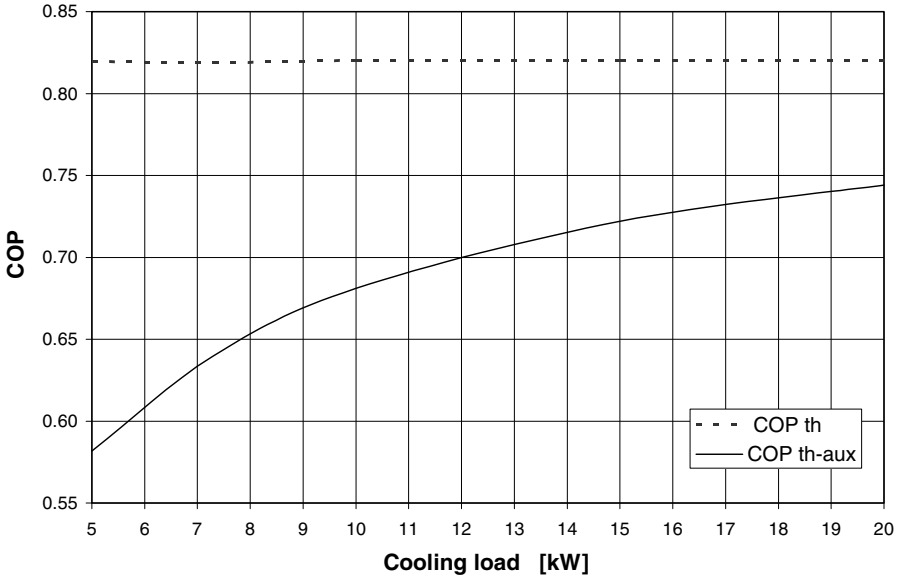


Fig. 12. Theoretical $COP_{th}$ and $COP_{th\text{-}aux}$ versus cooling load for second arrangement.

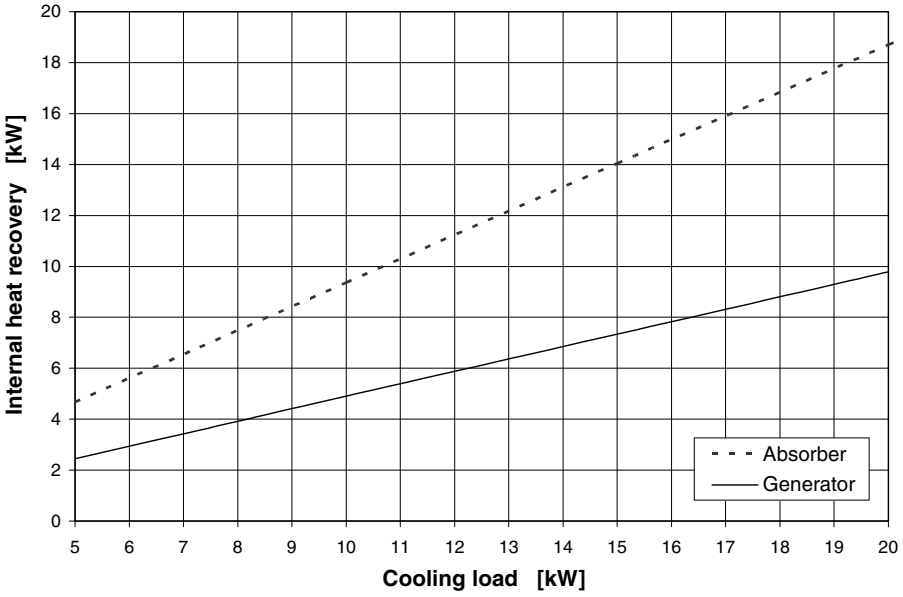


Fig. 13. Theoretical internal heat recovery versus cooling load for second arrangement.

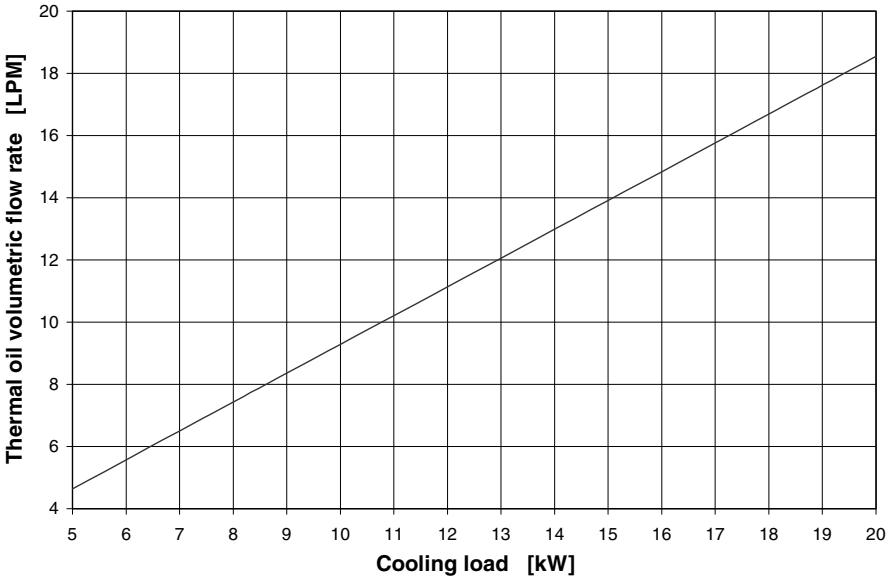


Fig. 14. Theoretical volumetric flow of the thermal oil versus cooling load.

the generator for an equal operation temperature of 290 °C, obtained from the exhaust gases.

As $COP_{th\text{-}aux}$ and the internal heat recovery $Q_{ir\text{-}ab}$ and $Q_{ir\text{-}ge}$ increase with an increase in the cooling capacity of the refrigeration system, the first law cogeneration efficiency $\eta_{I,cog}$ also increases as shown in Fig. 11, reaching values of 48% at the maximum cooling capacity of 25 kW, indicating a better use of the heat from the microturbine exhaust gases and lower exhaust gases rejected to the ambient. In the same way the cogeneration second law efficiency also increases, however, its values are lower than for the first law as it takes into account the destruction of exergy due to internal irreversibility effects, obtaining a value of 27.2% for a cooling load of 25 kW, Fig. 12, shows the values obtained for the coefficient of performance $COP_{th}$ and $COP_{th\text{-}aux}$ operating in the range of 5 kW up to 20 kW, which is the maximum cooling capacity obtained for configuration 4(b). It can be seen that the $COP_{th}$ values are in the order of 0.81 and are similar to ones obtained for the configuration shown in Fig. 4(a); however, the $COP_{th\text{-}aux}$ values vary from 0.56 to 0.74 and reach values which are 10% lower than those obtained with the other configuration, the reason being that the $COP_{th\text{-}aux}$ is affected by the heat losses in the recuperator, as an efficiency of 95% was considered. Fig. 13 shows how the internal heat recovery $Q_{ir\text{-}ab}$ and $Q_{ir\text{-}ge}$ increases as the

refrigeration capacity increases, in a similar form for this configuration 4(b) as it did in configuration 4(a). Fig. 14 shows the theoretical volumetric heating oil flow required to produce the cooling capacity from 5 to 20 kW, with a generator heating temperature $T_{ge}$ of 220 °C. Fig. 15 shows the second law cogeneration efficiency values $\eta_{II,cog}$ and how this value increases with an increase of the cooling capacity. The second law efficiency increases reaching a value of 26.7% at the maximum cooling load of 20 kW and its value departs from that of the first law efficiency as the cooling load is increased for a constant evaporation temperature due to the increment in entropy also increases the $Q_{EV}$, according to the definition of entropy by Kotas [19]; For this reason efficiencies lines in Fig. 15 have different slope. The results are similar for both configurations 4(a) and 4(b). Finally, Fig. 16 shows the useful heat from the turbine exhaust gases not recovered and rejected to the environment against the cooling capacity of the GAX system. Also shown are the exhaust gases temperature which is similar for both configurations studied.

## 5. Conclusions

The experimental tests developed were useful to validate the simulation model and to evaluate the performance of the GAX-PCS operated with thermal oil. The simulation model carried out can be used to predict the values of the operation parameters when the GAX-PCS is operated at

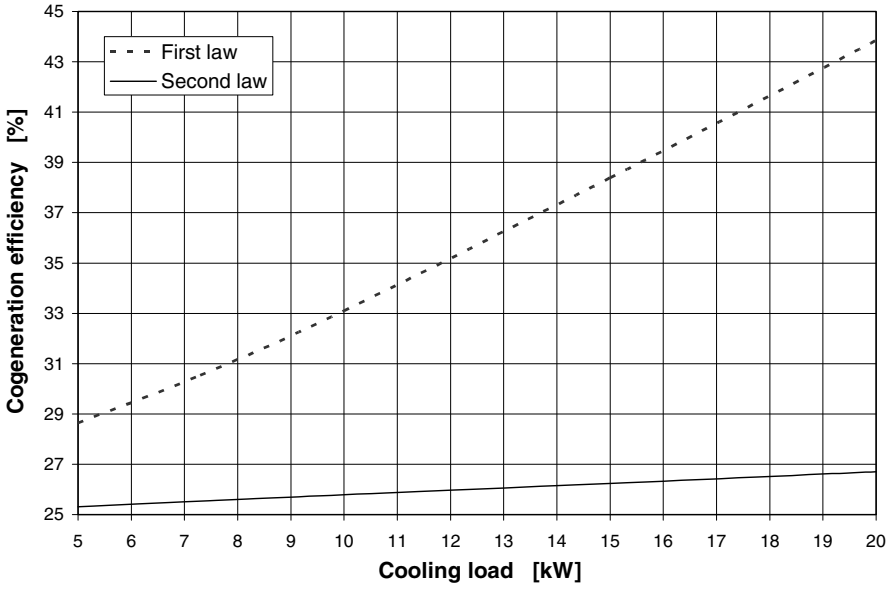


Fig. 15. Theoretical first and second law cogeneration efficiency versus cooling load for second arrangement.

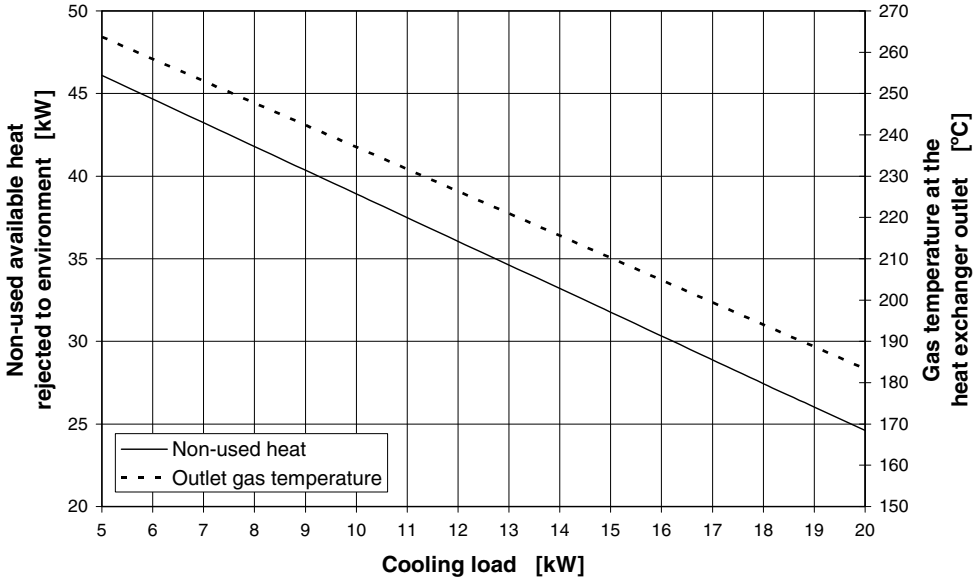


Fig. 16. Not used available heat reject to environment versus cooling load.

different working conditions. The real system was stabilized after 25–30 min of operation, obtaining a maximum cooling load of 7.1 kW. The $COP_{th}$ obtained was of 0.58 with a generation temperature of 192.5 °C. The experimental results were lower than the design results due to lower range of operating temperature of the heating oil and the low performance of the absorber of the prototype, but this problems that will be corrected in a second stage. The numerical simulations of a GAX absorption cooling system coupled to a MGT as a cogeneration system were analyzed. Two configurations were proposed; the configuration (a) with direct use of the exhaust gases in the GAX generator shows a $COP_{th\text{-}aux}$ 10% higher than configuration (b) with an extra heat exchanger between the thermal oil and the exhaust gases. For configuration (a) cogeneration and second law efficiency are 44% and 26.7%, respectively, and it is possible to obtain 5 kW more of cooling load that configuration (b). With this comparative analysis is possible to know the potential that these cogeneration systems could reach, recovering efficiently the disposed energy in the microturbine exhaust gases, improving the overall performance of the cogeneration systems.

## Acknowledgements

The authors thank for the financial support for this research work, through of CONACYT project U44764-Y. We are also grateful to Cesar García for yours useful comments to this work.

## References

[1] P.D. Fairchild, S.D. Labinov, A. Zaltash, B.D.T. Rizy, Experimental and theoretical study of microturbine-based BCHP system, in: ASME International Congress and Exposition, New York, 2001, pp. 11–16.
[2] Y. Hwang, Potential energy benefits of integrated refrigeration systems with microturbine and absorption chiller, International Journal of Refrigeration 27 (2004) 816–829.
[3] J.C. Bruno, A. Valero, A. Coronas, Performance analysis of combined microgas turbines and gas fired water/LiBr absorption chillers with post-combustion, Applied Thermal Engineering 25 (2005) 87–99.
[4] N. Velázquez, R. Best, Methodology for the energy analysis of an air cooled GAX absorption heat pump operated by natural gas and solar energy, Applied Thermal Engineering 22 (2002) 1089–1103.
[5] D. Zheng, W. Deng, H. Jin, J. Ji, $\alpha$–$h$ diagram and principle of exergy coupling of GAX cycle, Applied Thermal Engineering 27 (2007) 1771–1778.
[6] D.K. Priedeman, M.A. Garrabrant, J.A. Mathias, R.E. Stout, R.N. Christensen, Performance of a residential sized GAX absorption chiller, Transactions of the ASME 123 (2001) 236–241.
[7] E. Ozaki, T. Yumikura, A. Tsujimori, Performance of a residential ammonia–water absorption heat pump, ASME/JSME Thermal Engineering Conference 4 (1995) 607–612.
[8] K.E. Herold, R. Radermacher, S.A. Klein (Eds.), Absorption Chillers and Heats Pumps, CRC Press Inc., 1996.
[9] M.V. Rane, D.C. Erickson, Advanced absorption cycle: vapor exchange GAX, in: International Absorption Heat Pump Conference ASME, AES-Vol. 31, 1993, pp. 25–32.
[10] M.D. Staicovici, Polybranched regenerative GAX cooling cycles, International Journal of Refrigeration 18 (1995) 318–329.
[11] D. Kim, Advanced Regenerative Absorption Refrigeration Cycles, US Patent 4, 1990.
[12] Y.T. Kang, A. Akisawa, T. Kashiwagi, An advanced GAX cycle for waste heat recovery: WGAX cycle, Applied Thermal Engineering 19 (1999) 933–947.
[13] N. Velázquez, Estudio de sistemas de absorción avanzados para operar con gas natural asistido por energía solar. Ph.D. Thesis, Centro de Investigación en Energía de la Universidad Nacional Autónoma de México, México DF, 2002.
[14] V.H. Gómez, Simulación numérica y validación experimental de intercambiadores de calor de tubos aletados y placas, y su integración a un ciclo de refrigeración por absorción. Ph.D. Thesis (in process), Centro de Investigación en Energía de la Universidad Nacional Autónoma de México, Temixco, Morelos, México, 2007.
[15] A. Vidal, J.C. Bruno, R. Best, A. Coronas, Performance characteristics and modeling of a micro gas turbine for their integration with thermally activated cooling technologies, International Journal of Energy Research 32 (2007) 119–134.
[16] J.C. Ho, K.C. Chua, S.K. Chou, Performance study of a microturbine system for cogeneration application, Renewable Energy 29 (2004) 1121–1133.
[17] M.A. Smith, P.C. Few, Second law analysis of an experimental domestic scale cogeneration plant incorporating a heat pump, Applied Thermal Engineering 22 (2001) 93–110.
[18] P.M. Tchouate-Heteu, L. Bolle, Economie d'energie en trigeneration, International Journal of Thermal Sciences 41 (2002) 1151–1159.
[19] T.J. Kotas, The Exergy Method of Thermal Plant Analysis, Krieger Publish Company, Malabar, Florida, USA, 1995, pp. 97–106.
[20] D. Zheng, B. Chen, Y. Qi, H. Jin, Thermodynamic analysis of a novel absorption power/cooling combined cycle, Applied Energy 83 (2006) 311–323.
[21] Refprop version 7.0 Reference Fluid Thermodynamic and Transport Properties, NIST Standard Reference Database 23, 2002.
[22] A. Vidal, R. Best, R. Rivero, J. Cervantes, Analysis of a combined power and refrigeration cycle by the exergy method, Energy 31 (2006) 3401–3414.
[23] S.P. Verma, J. Andaverde, E. Santoyo, Application of the error propagation theory in estimates of static formation temperatures in geothermal and petroleum boreholes, Energy Conversion and Management 47 (2006) 3659–3671.